Research Article

Abdul Hamid Ganie, Muhammad Farooq, Mohammad Khalid Nasrat*, Muhammad Bilal, Taseer Muhammad, Kaouther Ghachem, and Adnan

Radiative nanofluid flow over a slender stretching Riga plate under the impact of exponential heat source/sink

https://doi.org/10.1515/phys-2024-0020
received January 10, 2024; accepted March 16, 2024

Abstract: Recognizing the flow behaviours across a Riga plate can reveal information about the aerodynamic efficiency of aircraft, heat propagation, vehicles, and other structures. These data are critical for optimizing design and lowering drag. Therefore, the purpose of the current analysis is to examine the energy and mass transfer across the mixed convective nanofluid flows over an extending Riga plate. The fluid flow is deliberated under the influences of viscous dissipation, exponential heat source/sink, activation energy, and thermal radiation. The Buongiorno's concept is utilized for the thermophoretic effect and Brownian motion along with the convective conditions. The modelled are simplified into the lowest order by using similarity transformation. The obtained set of non-dimensional ordinary differential equations is then numerically solved through the parametric continuation method. For accuracy and validation of the outcomes, the results are compared to the existing studies. From the graphical analysis, it can be observed that the fluid velocity boosts with the rising values of the divider thickness parameter. The fluid temperature also improves with the effect of Biot number, Eckert number, and heat source factor. Furthermore, the effect of heat source sink factor drops the fluid temperature.

Keywords: thermal radiation, viscous dissipation, numerical solution, mixed convection, exponential heat source/sink, slender sheet

*** Corresponding author: Mohammad Khalid Nasrat,** Department of Physics, Laghman University, Mehtarlam City, 2701, Laghman, Afghanistan, e-mail: khalid.nasrat@lu.edu.af
Abdul Hamid Ganie: Department of Basic Science, College of Science and Theoretical Studies, Saudi Electronic University, Riyadh, 11673, Saudi Arabia
Muhammad Farooq, Muhammad Bilal: Sheikh Taimur Academic Block-II, Department of Mathematics, University of Peshawar, 25120, Khyber Pakhtunkhwa, Pakistan
Taseer Muhammad: Department of Mathematics, College of Science, King Khalid University, Abha, Saudi Arabia
Kaouther Ghachem: Department of Industrial Engineering and Systems, College of Engineering, Princess Nourah Bint Abdulrahman University, P.O. Box 84428, Riyadh, 11671, Saudi Arabia
Adnan: Department of Mathematics, Mohi-ud-Din Islamic University, Nerian Sharif, AJ and K, 12080, Pakistan

Nomenclature

$T_w(x)$	surface temperature
y	sheet thickness
α_1	thermal diffusivity
D_B	Brownian diffusion
β_T	thermal gradients factor
E_a	activation energy
Kr	chemical reaction
c_p	specific heat
Nt	thermophoresis term
λ_C	fixation lightness factor
β_1	dimensionless term
Q_e	heat source/sink factor
Q	modified Hartman number
Ec	Eckert number
VD	viscous dissipation
C_{fx}	shear stress
$U_w(x)$	uniform velocity of Riga plate
2D	two-dimensional
υ	kinematic viscosity
$C_w(x)$	surface concentration
K	thermal conductivity
τ	thermal capacity
j_0	current density
D_T	thermophoresis diffusion
λ_T	lightness parameter
β_C	concentration expansion factor
K_c	factor of chemical reaction
Sc	Schmidt number
Bi	Biot number

Nb	Brownian constant
Sh_x	Sherwood number

1 Introduction

The study of the fluid flow over a Riga plate contributes to the development of techniques for controlling boundary layer disparity, which is critical for enhancing the efficiency of multiple engineering systems and reducing drag force. Recognizing the flow behaviours across a Riga plate can reveal information about the aerodynamic efficiency of aircraft, vehicles, and other structures. These data are critical for optimizing design and lowering drag. Researchers may enhance heat conduction and thermal proficiency by analyzing the heat exchange features of fluid flow across a Riga plate [1–3]. Abdul Hakeem *et al.* [4] numerically simulated the three-dimensional (3D) flow of nanofluids containing aluminium oxide (Al_2O_3) and magnetite (Fe_3O_4) nanoparticles through a Riga plate. It was found that the radiation parameter increases the efficiency of energy transportation. Ishtiaq *et al.* [5] investigated the rate-type fluid under the effect of heat radiation on passing within a Riga plate and concluded that arising Prandtl numbers decrease the temperature curve, whereas higher radiation factor increases the temperature curve. Asogwa *et al.* [6] assessed the mass and energy transportation phenomena caused by the parabolic fluid flow on an upward extending Riga surface. The Hartmann number has a momentous impression on fluid flow, as observed with the involvement of the Riga sheet. Adnan *et al.* [7] studied the thermal features of a water-based nano liquid containing oxide and metallic nanoparticles (SiO_2, Au, MoS_2) through a cylinder under combined convection. The study found that increasing the quantity of MoS_2 tiny particles from 0.1 to 0.5%, as well as the Eckert number, significantly improved the fluidity of the functional fluid. Bani-Fwaz *et al.* [8] evaluated the nanofluid thermal transfer characteristics within a channel generated by expanding and contracting walls. The velocity of stretching walls is measured at its maximum in the channel centre. Waqas *et al.* [9] and Hamad *et al.* [10] reported the mass and energy transference within nano liquid flow across a tilted prolonging sheet, under the upshot of magnetic fields and chemical reactions. The fluid velocity was found to increase with the change of the Tangent fluid parameter and Richardson numbers. Some further results are reported by refs. [11–14].

Thermal radiation pertains to the mechanism of heat transfer *via* electromagnetic waves emitted by a fluid due to its temperature. When a fluid (like a liquid or a gas) is heated, its molecules gain energy and move more rapidly. As a result, these molecules emit electromagnetic radiation, primarily in the form of infrared radiation. This thermal radiation process is one of the ways heat is conveyed from a fluid to its ambiance or from one part of the fluid to another. It is crucial to observe that while thermal radiation can occur in a fluid, it is not exclusive to fluids and can also happen in solids and a vacuum [15]. Jamshed *et al.* [16] conducted an in-depth exploration of the time-dependent nanoliquid focusing on its entropy characteristics and thermal transport. Abbas *et al.* [17] focused on investigating heat transference and fluid motion across an inclined movable surface particularly examining the Sakiadis flow, while their analysis included factors like changing density, thermal radiation, and magnetization. Yu and Wang [18] presented the dynamics of heat and fluid flow between two spinning and stretching disks submerged in a water-based fluid containing carbon nanotubes, and their findings indicated that elevated Reynolds number (Re) values result in a diminution in the velocity near the disk surfaces considering thermal radiation as well. Sneha *et al.* [19] and Salawu *et al.* [20] scrutinized the impact of hydromagnetic flow consisting of CNTs. The study unveiled that enhancing the volume fraction of hybrid nanoparticles contributes to improved energy optimization of the system. Some prominent and recent literature regarding thermal radiation effects have been highlighted in refs. [21–26].

Exponential heat sources/sinks (EHSS) are widely used in heat transport analysis to simulate a variety of physical phenomena. EHSS can be used in thermal management, geothermal energy systems, nuclear reactor design, and environmental studies [27–29]. Elangovan *et al.* [30] debated the impact of HSS on the fluid flow across a channel with an irregular wall temperature. The results show that the electromagnetic radiation factor reduces temperature, while the higher Brinkman number causes temperature to increase. Nabwey *et al.* [31] and Maranna *et al.* [32] evaluated the impacts of EHSS on the 2D flow of Walter's B and second-grade ternary nanofluids across a porous reducing the flat substrate. Hussain *et al.* [33] assessed the HSS, buoyancy impacts, and heat transport through an upward flat surface in a Darcy porous media. The results showed that the boundary effect speeds up because of the superior effect of the permeation variable. Adnan *et al.* [34] proposed a nanofluid model based on ZnO-SAE50, the nano-lubricant, with the additional impacts of thermal radiations, EHSS, and resistive heating and magnetic field. The results show that employing ZnO-SAE50 nano-lubricant maximizes heat transportation, whereas traditional SAE50 fails to accomplish the ideal heat exchange rate. Some valuable updated results are presented by refs. [35–39].

The objective of the current analysis is to examine the energy and mass transfer across the mixed convective nanofluid flows over an extending Riga plate. By recognizing the flow behaviours across a Riga plate can reveal information about the aerodynamic efficiency of aircraft, heat propagation, vehicles, and other structures. These data are critical for optimizing design and lowering drag. The fluid flow is studied under the influences of viscous dissipation, EHSS, activation energy, and thermal radiation. The modelled are simplified into the lowest order by using similarity transformation, which is numerically solved through the parametric continuation method (PCM). For accuracy and validation of the outcomes, the outcomes are equated to the existing studies. In the next portion, the problem is mathematically designed and solved

2 Mathematical formulation

The 2D incompressible fluid flow across a vertical heated Riga plate is considered. The permanent alternating anodes and magnetization are employed by the Riga plate towards the x-axis as demonstrated in Figure 1. The flow is induced by the stretching plate along the y-axis. The plate is supposed to be moving with uniform velocity $U_w(x)$. The thickness of sheet is defined as $y = A(x + b)^{\frac{(1-m)}{2}}$, where $m \neq 1$ and A is a constant that defines the sheet stretching. The surface temperature and mass are expressed as $T_w(x) = A_1(x + b)^r$ and $C_w(x) = A_2(x + b)^s$. The 2D incompressible flow based on the aforementioned presumptions are stated as follows [40–42]:

$$\frac{\partial u}{\partial x} = -\frac{\partial v}{\partial y}, \tag{1}$$

$$u\frac{\partial u}{\partial x} + v\frac{\partial u}{\partial y} - \upsilon\frac{\partial^2 u}{\partial y^2} = \frac{\pi j_0 M_0}{8\rho}\exp\left(\frac{-\pi}{a_1 x}y\right) + g(T - T_\infty)\beta_T + g(C - C_\infty)\beta_C, \tag{2}$$

$$u\frac{\partial T}{\partial x} + v\frac{\partial T}{\partial y} - \alpha_1\frac{\partial^2 T}{\partial y^2} = \tau\left[D_B\frac{\partial C}{\partial y}\frac{\partial T}{\partial y} + \frac{D_T}{T_\infty}\left(\frac{\partial T}{\partial y}\right)^2\right] + \frac{1}{(\rho C_p)_f}\frac{4\sigma^*}{3k^*}\frac{\partial^2}{\partial z^2}(4T_\infty^3 T) + \frac{Q_e^*}{(\rho C_p)_f}(T - T_\infty)\exp\left(-\sqrt{\frac{a}{\upsilon_f}}ny\right) + \frac{\mu}{(\rho C_p)_f}\left(\frac{\partial u}{\partial y}\right)^2, \tag{3}$$

$$u\frac{\partial C}{\partial x} + v\frac{\partial C}{\partial y} = D_B\left(\frac{\partial^2 C}{\partial y^2}\right) + \frac{D_T}{T_\infty}\left(\frac{\partial^2 T}{\partial y^2}\right) - k_r^2(C - C_0)\left(\frac{T}{T_\infty}\right)^n \exp\left(-\frac{E_a}{\kappa T}\right). \tag{4}$$

The boundary conditions (BCs) are as follows:

$$\left.\begin{aligned} &u = U_0(x + b)^m = U_w(x),\\ &v = 0 - K\left(\frac{\partial T}{\partial y}\right) = h_s(x)(T_w - T),\\ &D_B\left(\frac{\partial C}{\partial y}\right) = -\left(\frac{D_T}{T_\infty}\right)\frac{\partial T}{\partial y}, \end{aligned}\right\} \text{at } y = A(x + b)^{\frac{(1-m)}{2}}$$

$$u \to U_e(x) = U_\infty(b + x)^m, \quad C \to C_\infty, \quad T \to T_\infty\} \text{ as } y \to \infty. \tag{5}$$

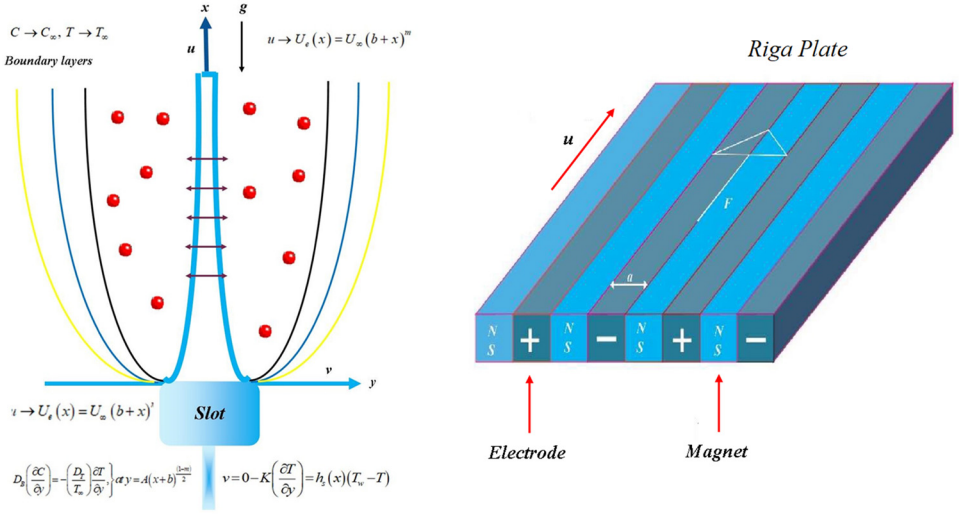

Figure 1: Physical illustration of stretching sheet and Riga plate.

The variable magnetization, changing width of magnets and electrodes, and heat transfer are stated as follows:

$$\left[M_0(x) = M_0(x+b)^{2m-1},\ K_1(x) = K_1(x+b)^{(m-1)},\right.$$
$$\left.a_1(x) = a_1(x+b)^{\frac{(1-m)}{2}},\ h_s(x) = h_s(x+b)^{\frac{(1-m)}{2}}\right]. \tag{6}$$

The non-dimensional variables are expressed as follows [43]:

$$\eta = y\sqrt{\frac{U_0(x+b)^{m-1}}{\upsilon}\frac{(m+1)}{2}},\quad \Theta(\eta) = \frac{T-T_\infty}{T_w-T_\infty},$$
$$\psi = \sqrt{U_0(x+b)^{(m+1)}\upsilon\frac{2}{m+1}}F(\eta),\quad \Phi(\eta) = \frac{C-C_\infty}{C_w-C_\infty}. \tag{7}$$

The velocity and stream function components are as follows:

$$v = -\frac{\partial\psi}{\partial x} = -\sqrt{\upsilon_\infty\frac{2}{m+1}U_0(x+b)^{(m-1)}}\left[\frac{(m-1)\eta}{2}F'(\eta)\right.$$
$$\left.+\frac{m+1}{2}F(\eta)\right], \tag{8}$$
$$u = \frac{\partial\psi}{\partial y} = U_0(x+b)^m F'(\eta).$$

The insertion of Eqs. (7) and (8) in Eqs. (1)–(5) are stated as follows:

$$F''' + FF'' - \left(\frac{2m}{(m+1)}\right)(F')^2 + \left(\frac{2}{(m+1)}\right)Qe^{-(\beta_1\eta)}$$
$$+\left(\frac{2}{(m+1)}\right)\lambda_T(\Theta + \lambda_C\Phi) = 0, \tag{9}$$

$$(1+\mathrm{Rd})\Theta'' + \mathrm{Pr}\Theta'(\mathrm{Nb}\Theta' + \mathrm{Nt}\Theta' + F)$$
$$-\frac{2\mathrm{Pr}}{m+1}((2m-1)F'\Theta) \tag{10}$$
$$+Q_e\exp(-n\eta) + \mathrm{PrEc}(F'')^2 = 0,$$

$$\Phi'' + \left(\frac{\mathrm{Nt}}{\mathrm{Nb}}\right)\Theta'' - \frac{2(2m-1)}{(m+1)}\mathrm{Sc}\,F'\Phi + \mathrm{Sc}\,F\Phi'$$
$$-\mathrm{Sc}\,K_c(1+\delta\theta)^n\Phi\exp\left(-\frac{E}{1+\delta\theta}\right) = 0. \tag{11}$$

The BCs for the reduced system of ODEs are follows:

$$\frac{F(\alpha)}{\alpha} - \frac{(1-m)}{(1+m)} = 0,\quad \Theta'(\alpha) = -\mathrm{Bi}(1-\Theta(\alpha)),$$
$$F'(\alpha) = 1,$$
$$\Theta'(\alpha) = -\frac{\mathrm{Nt}}{\mathrm{Nb}}\Theta'(\alpha),\quad F'(\infty)\to 0,\quad \Phi(\infty)\to 0, \tag{12}$$
$$\Theta(\infty)\to 0.$$

The non-dimensional parameters obtained from Eqs. (9)–(11) are defined in the following table.

Parameters	Symbols	Expression
Thermal Grashof number	λ_T	$\lambda_T = \pm\frac{g\beta A_1}{U_0^2}$
Mass Grashof number	λ_C	$\lambda_C = \pm\frac{g\beta_C A_2}{U_0^2}$
Thermophoresis factor	Nt	$\mathrm{Nt} = \frac{\tau D_T(T_w-T_\infty)}{T_\infty\upsilon}$
Schmidt number	Sc	$\mathrm{Sc} = \frac{\upsilon}{D_B}$
Heat source/sink parameter	Q_e	$Q_e = \frac{Q_e^* l}{a(\rho C_p)_f}$
Dimensionless constant	β_1	$\beta_1 = \frac{\pi}{a_1}\sqrt{\frac{2}{(m+1)}\frac{\upsilon}{U_0}}$
Eckert number	Ec	$\mathrm{Ec} = \frac{U_w^2}{c_p(T_w-T_\infty)}$
Chemical reaction factor	K_c	$K_c = \frac{K_1}{U_0}$
Thermal radiation factor	Rd	$\mathrm{Rd} = \frac{16\sigma^{**}T_\infty^3(T_w-T_\infty)}{3k^*k}$
Brownian motion	Nb	$\mathrm{Nb} = \frac{\tau D_B(C_w-C_\infty)}{\upsilon}$
Divider thickness term	α	$\alpha = A\sqrt{\frac{U_0(m+1)}{2\upsilon}}$
Modified Hartman number	Q	$Q = \frac{\pi j_0 M_0}{8\rho_\infty U_0^2}$
Biot number	Bi	$\mathrm{Bi} = \frac{h_s}{k}\sqrt{\frac{2}{(m+1)}\frac{\upsilon}{U_0}}$

Further, we are introducing $\Theta(\eta) = \theta(\eta-\alpha) = \theta(\xi)$, $F(\eta) = f(\eta-\alpha) = f(\xi)$, where $\eta = \alpha$ illustrate the flat surface. We obtain:

$$f''' + ff'' - \frac{2m(f')^2}{(m+1)} + \frac{2}{(m+1)}Qe^{-\beta_1(\xi+a)}$$
$$+\frac{2}{(m+1)}(\lambda_T\theta + \lambda_C\varphi) = 0, \tag{13}$$

$$(1+\mathrm{Rd})\theta'' + \mathrm{Pr}\theta'(\mathrm{Nb}\varphi' + \mathrm{Nt}\theta' + f) + Q_e\exp(-n\eta)$$
$$+\mathrm{PrEc}(f'')^2 - \frac{2\mathrm{Pr}}{(m+1)}((2m-1)f'\theta) = 0, \tag{14}$$

$$\varphi'' + \left(\frac{\mathrm{Nt}}{\mathrm{Nb}}\right)\theta'' - \frac{2(2m-1)}{(m+1)}\mathrm{Sc}\,f'\varphi + \mathrm{Sc}\,f\varphi'$$
$$-\mathrm{Sc}\,K_c(1+\delta\theta)^n\Phi\exp\left(-\frac{E}{1+\delta\theta}\right) = 0. \tag{15}$$

The final BCs are given as follows:

$$\frac{f(0)}{\alpha} - \frac{(1-m)}{(1+m)} = 0,\quad \mathrm{Nb}\,\varphi'(0) = -\mathrm{Nt}\,\theta'(0),$$
$$f'(0) = 1,\quad \frac{\theta(0)}{1-\theta(0)} = -\mathrm{Bi}, \tag{16}$$
$$f'(\infty)\to 0,\quad \varphi(\infty)\to 0,\quad \theta(\infty)\to 0.$$

The shear stress C_{fx}, Nusselt number Nu_x, and Sherwood number Sh_x can be defined as follows:

$$C_{fx} = \left(\frac{1}{U_w^2}\right)\tau_w, \quad Sh_x = \left(\frac{(x+b)}{(C_w - C_\infty)}\right)j_w, \quad Nu_x = \left(\frac{(x+b)}{(T_w - T_\infty)}\right)q_w, \tag{17}$$

where $\tau_w = \upsilon\frac{\partial u}{\partial y}$, $j_w = \frac{\partial C}{\partial y}$ and $q_w = \frac{\partial T}{\partial y}$ at $y = A(x+b)^{\frac{(1-m)}{2}}$.

The dimensionless form of Eq. (17) is obtained as follows:

$$Re_x^{1/2}C_{fx} = \left(\frac{m+1}{2}\right)^{1/2} f''(0), \quad Re_x^{-1/2}\,Sh_x = -\left(\frac{m+1}{2}\right)^{1/2}\varphi'(0),$$
$$Re_x^{-1/2}\,Nu_x = -\left(\frac{m+1}{2}\right)^{1/2}\theta'(0).$$

3 Numerical solution

The PCM is a numerical method, which can be applied to almost all sorts of complex problems, such as problems of nonlinear mechanics, thermo-fluids, Newtonian and Non-Newtonian fluids models, and inverse problems [44–46]. The detailed steps of PCM are defined as follows:

Step 1: In this step, the system of ODEs is reduced to its lowest order.

$$\left.\begin{aligned} &\varpi_1(\eta) = f(\eta),\ \varpi_3(\eta) = f''(\eta),\ \varpi_5(\eta) = \theta'(\eta),\\ &\varpi_7(\eta) = \varphi'(\eta),\\ &\varpi_2(\eta) = f'(\eta),\ \varpi_4(\eta) = \theta(\eta),\ \varpi_6(\eta) = \varphi(\eta) \end{aligned}\right\}. \tag{18}$$

By placing Eq. (18) in Eqs. (13)–(15), we obtain:

$$\varpi_3' + \varpi_1\varpi_3 - \frac{2m}{(m+1)}(\varpi_2)^2 + \frac{2}{(m+1)}Qe^{-\beta_1(\xi+a)} + \frac{2}{(m+1)}\lambda_T(\varpi_4 + \lambda_C\varpi_6) = 0, \tag{19}$$

$$(1+Rd)\varpi_5' + Pr\,\varpi_5(Nb\,\varpi_7 + Nt\,\varpi_5 + \varpi_1) + Q_e\exp(-n\eta) + Pr\,Ec(\varpi_3)^2 - \frac{2Pr}{(m+1)}((2m-1)\varpi_2\,\varpi_4) = 0, \tag{20}$$

$$\varpi_7' + \left(\frac{Nt}{Nb}\right)\varpi_5' - \frac{2(2m-1)}{(m+1)}Sc\,\varpi_2\,\varpi_6 + Sc\,\varpi_1\varpi_7 - Sc\,K_c(1+\delta\varpi_4)^n\varpi_6\exp\left(-\frac{E}{1+\delta\varpi_4}\right) = 0. \tag{21}$$

The BCs for the first-order ODEs are as follows:

$$\frac{\varpi_1(0)}{a} - \frac{(1-m)}{(1+m)} = 0, \quad Nb\,\varpi_7(0) = -Nt\,\varpi_5(0), \quad \varpi_2(0) = 1, \quad \frac{\varpi_4(0)}{1-\varpi_4(0)} = -Bi, \quad \varpi_2(\infty)\to 0, \quad \varpi_6(\infty)\to 0, \quad \varpi_4(\infty)\to 0. \tag{22}$$

Step 2: Presenting parameter p in Eqs. (20)–(22):

$$\varpi'_3 + \varpi_1(\varpi_3 - 1)p - \frac{2m}{(m+1)}(\varpi_2)^2 + \frac{2}{(m+1)}Qe^{-\beta_1(\xi+a)} + \frac{2}{(m+1)}\lambda_T(\varpi_4 + \lambda_C\,\varpi_6) = 0, \tag{23}$$

$$(1+Rd)\varpi'_5 + Pr(\varpi_5 - 1)p(Nb\,\varpi_7 + Nt\,\varpi_5 + \varpi_1) + Q_e\exp(-n\eta) + Pr\,Ec(\varpi_3)^2 - \frac{2Pr}{(m+1)}((2m-1)\varpi_2\,\varpi_4) = 0, \tag{24}$$

$$\varpi'_7 + \left(\frac{Nt}{Nb}\right)\varpi'_5 - \frac{2(2m-1)}{(m+1)}Sc\,\varpi_2\,\varpi_6 + Sc\,\varpi_1(\varpi_7 - 1)p - Sc\,K_c(1+\delta\varpi_4)^n\varpi_6\,\exp\left(-\frac{E}{1+\delta\varpi_4}\right) = 0. \tag{25}$$

Step 3: By applying the numerical implicit scheme.

$$\left.\begin{aligned} &\frac{U^{i+1} - U^i}{\Delta\eta} = AU^{i+1}, \quad \frac{W^{i+1} - W^i}{\Delta\eta} = AW^{i+1},\\ &\text{or} \quad (I - \Delta\eta A)W^{i+1} = W^i \end{aligned}\right\}. \tag{26}$$

Finally, we obtain the iterative form as follows:

$$\left.\begin{aligned} &U^{i+1} = (I - \Delta\eta A)^{-1}U^i,\\ &W^{i+1} = (I - \Delta\eta A)^{-1}(W^i + \Delta\eta R) \end{aligned}\right\}. \tag{27}$$

Further, the discretized form is numerically solved through Matlab software.

Table 1 reveals the evaluation of the present work with the existing studies. It has been perceived from Table 1 that the PCM outcomes are reliable and accurate.

Table 1: Validation of the present results with published studies

A	*m*	Vaidya *et al.* [43]	Fang *et al.* [47]	Prasad *et al.* [48]	Present results
0.2	−0.3	0.0689	0.0723	0.0812	0.08124245
	−0.2	0.3011	0.5000	0.5000	0.5000021
	1.0	1.0511	1.0614	1.0524	1.0524468
	3.0	1.1003	1.0905	1.0905	1.0905843
	4.0	1.1166	1.1176	1.1166	1.1166686
0.4	−0.4	1.1645	1.1647	1.1645	1.1645123
	−0.2	1.0000	1.0000	1.0000	1.0000986
	1.0	1.0134	1.0214	1.0214	1.0214543
	2.0	1.0358	1.0359	1.0358	1.0358086
	4.0	1.0486	1.0466	1.0466	1.0466432

4 Results and discussion

The energy and mass transfer across the mixed convective nanofluid flows over an extending Riga plate is reported in the current analysis. The fluid flow is studied under the influences of viscous dissipation, EHSS, activation energy, and thermal radiation. The Buongiorno's concept is utilized for the thermophoretic effect and Brownian motion. The results obtained through PCM are presented through figures.

Figures 2–6 display the behaviour of velocity curve $f'(\eta)$ versus the divider thickness parameter a, power index of velocity m, Hartmann number Q, thermal Grashof number λ_T, and mass Grashof number λ_C, respectively. Figure 2 illustrates that fluid velocity boosts with the mounting values of divider thickness factor a. Physically, the sheet distending velocity increases and fluid viscosity lessens with the enhancing outcome of a, as a result, such phenomena are observed. Figures 3 and 4 specify that fluid velocity declines with the variation of m, although evolving with the impact of Q. The velocity field is the reducing function of Q, however, in the current incident; the flow stream improves due to magnetic impact. Figures 5 and 6

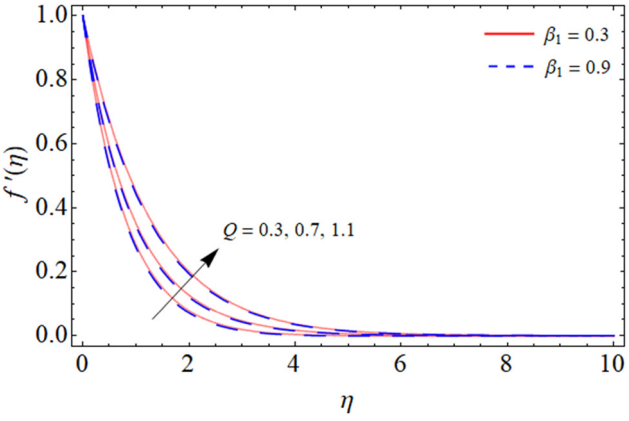

Figure 4: Velocity profile against modified Hartmann number Q.

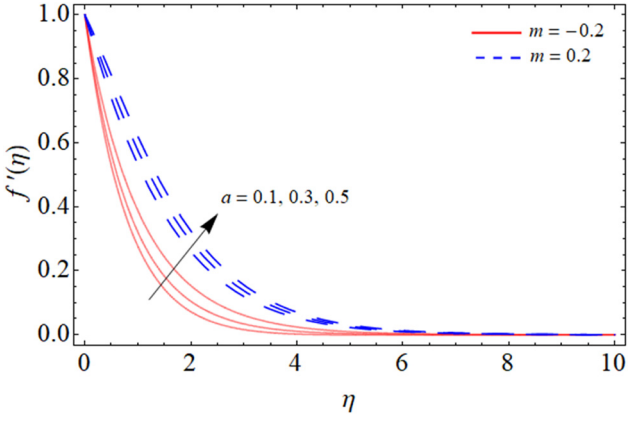

Figure 2: Velocity profile against divider thickness factor a.

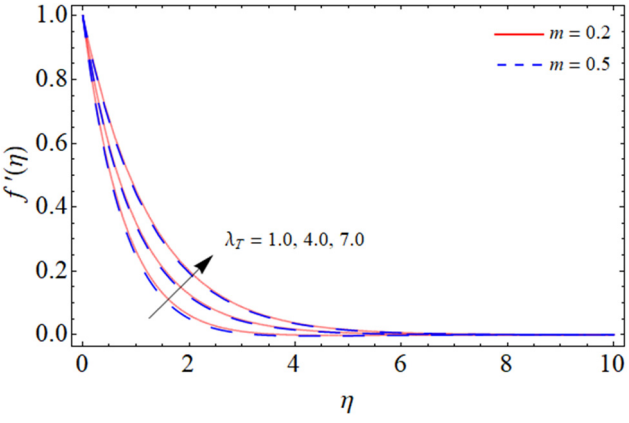

Figure 5: Velocity profile against λ_T.

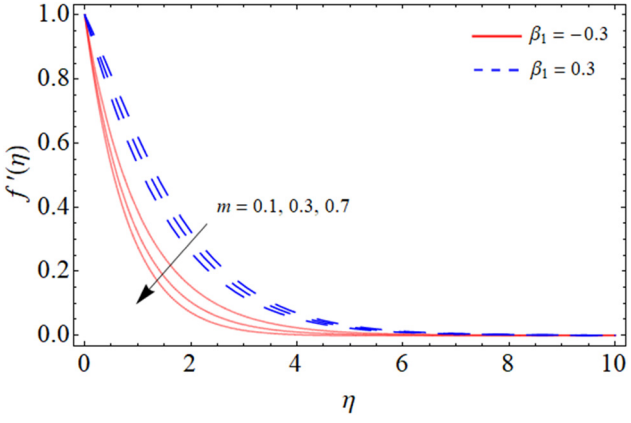

Figure 3: Velocity profile against power index m.

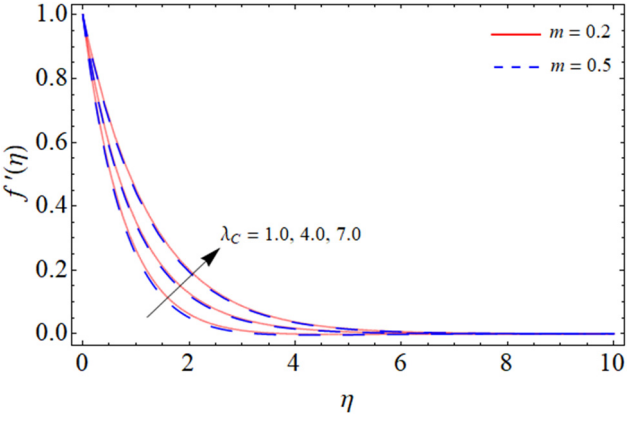

Figure 6: Velocity profile against λ_C.

entitle the significances of λ_C and λ_T on the fluid velocity, respectively. In fact, the positive variation of λ_T assistant to the flow, whereas the negative variation of λ_T disclose the conflicting behaviour. Moreover, the gravitational force turns into more active and stretching rate of surface drops, which results in such scenarios as revealed in Figures 5 and 6.

Figures 7–11 depict the nature of Rd, Bi, Eckert number Ec, Nt, and Q_e, respectively, on the $\theta(\eta)$. Physically, the thermal radiation variable enhances fluid temperature by transferring thermal energy *via* electromagnetic radiation generated by the fluid. When the thermal radiation variable rises, additional heat passes through *via* radiation, increasing the fluid temperature. This factor impacts the rate at which heat passes within the fluid and its surrounding environment, which in turn affects the fluid's overall temperature (Figure 7). The viscosity of the fluid dispels during flow into the kinetic energy, which increases the temperature of the fluid, and is known as viscous dissipation as displayed in Figure 8. Figure 9 reveals the effect of Bi on the thermal profile. It can be seen that the fluid temperature augments with the effect of Bi. Figure 10 demonstrates the effect of the thermophoresis term Nt on

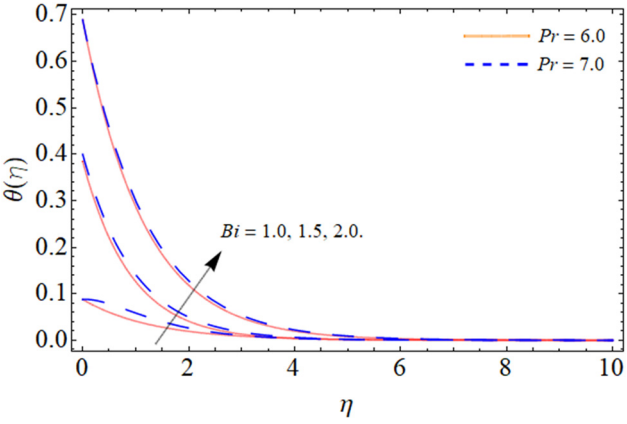

Figure 9: Thermal profile against Biot number Bi.

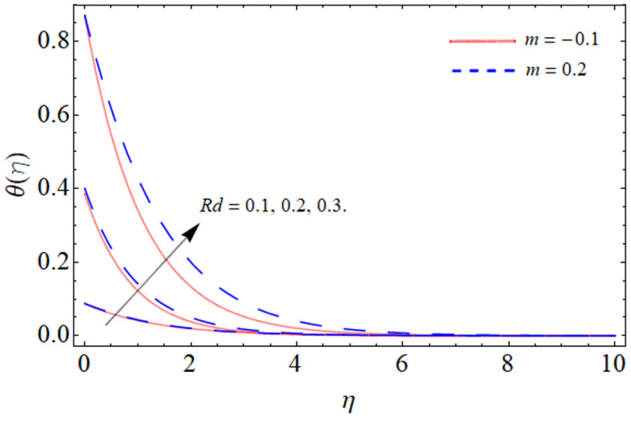

Figure 7: Thermal profile against heat radiation Rd.

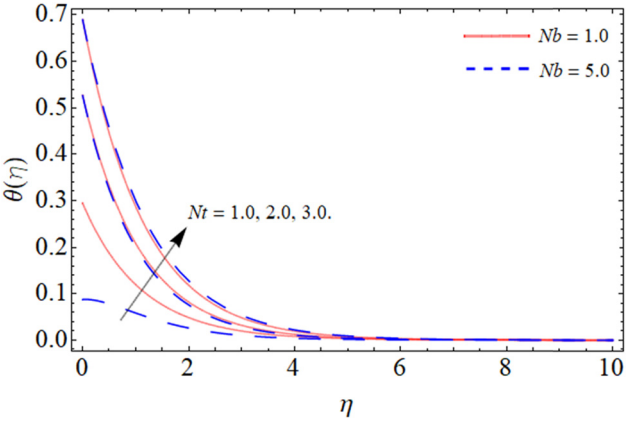

Figure 10: Thermal profile against thermophoresis Nt.

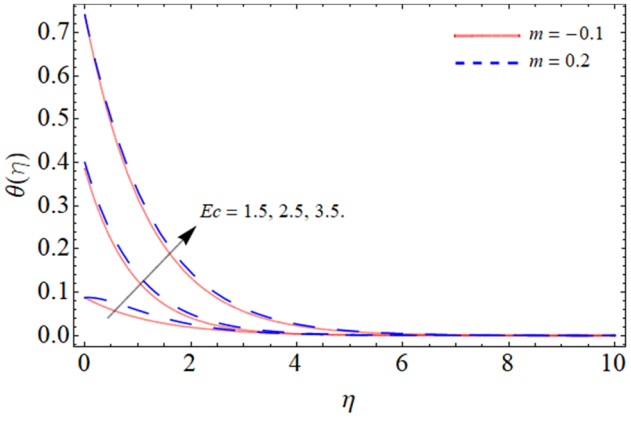

Figure 8: Thermal profile against Eckert number Ec.

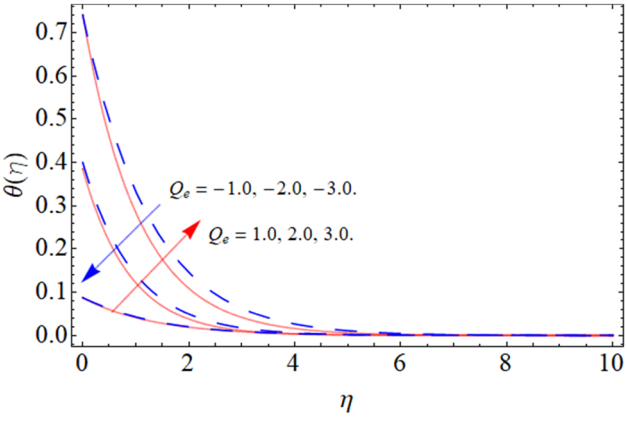

Figure 11: Thermal profile against heat source/sink Q_e.

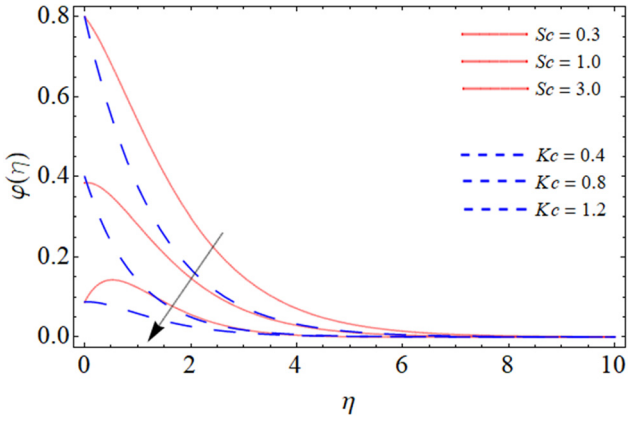

Figure 12: Mass curve against chemical reaction Kc and Schmidth number Sc.

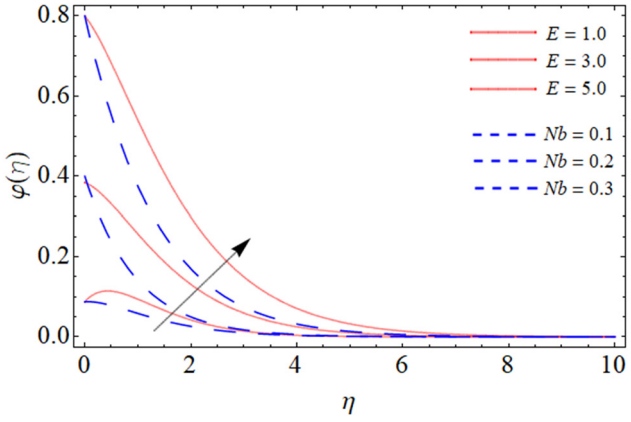

Figure 13: Mass curve against Brownian motion Nb and Activation energy *E*.

the heat profile $\theta(\eta)$. The implication of Nt intensifies the $\theta(\eta)$ as shown in Figure 10. The thermophoresis factor elevates fluid temperature by causing atoms in a fluid to migrate to higher temperatures areas. The motion of elements can cause a rise in the temperature inside the fluid as they develop in hotter areas. The thermophoresis term influences the temperature transportation inside the fluid. Figure 11 displays the impact of Q_e on the energy field. The impact of Q_e on increasing fluid temperature is caused by the introduction of heat energy into the system, which raises the fluid temperature. When heat is introduced to a fluid *via* a heat source, the temperature of the fluid rises as the energy is consumed. On the other hand, the heat sink variable reduces fluid temperature through eliminating heat energy from the system. Heat sinks act as a process to remove excess heat from the fluid, causing the temperature to drop. As a result, heat source factor increase the fluid temperature by adding heat energy, whereas heat sink parameters decrease fluid temperature through expelling heat energy from the system. Figure 12 clarifies the importance of Kr and Sc on the concentration field $\varphi(\eta)$. The impacts of both terms lessen the mass profile. The dissemination ratio is concentrated with the effect of Sc, which falls the mass transport as exposed in Figure 12. Likewise, the outcome of Kc declines the mass conduction rate $\varphi(\eta)$. Figure 13 regulates the effect of Nb and E on the $\varphi(\eta)$. Physically, the smallest volume of energy requisite for a chemical reaction is named as activation energy. So, the effect of E speed up the mass distribution rate as revealed in Figure 13. Similarly, the effect of Nb also increases the mass diffusion rate $\varphi(\eta)$.

Table 2 discloses the numerical outcomes for shear stress, Nusselt number, and Sherwood number. It can be remarked that the intensifying values of Kr and Pr augment the rate of energy and velocity transmission. The Ec has the similar behaviour as Kr and Pr, though drops the mass conveyance rate.

5 Conclusions

The fluid flow across a Riga plate has several applications in the field of aerodynamic efficiency of aircraft, automobiles, and heat propagation. Therefore, the energy and mass transfer across the mixed convective nanofluid flows over an extending Riga plate are reported in the current analysis. The fluid flow is studied under the influences of viscous dissipation, EHSS, activation energy, and thermal radiation. The modelled are simplified into lowest order by using similarity transformation, which are numerically solved through the PCM. From the graphical analysis, the following findings are deducted:

- The fluid velocity boosts with the mounting values of divider thickness parameter *a*.
- The fluid velocity declines with the variation of *m*, although evolving with the impact of *Q*.
- The positive variation of λ_T enhances the flow, whereas the negative variation of λ_T discloses the conflicting behaviour.
- The thermal radiation variable enhances fluid temperature by transferring thermal energy *via* electromagnetic radiation generated by the fluid.
- The effect of heat source sink parameter drops the energy field.
- The impacts of Kr and Sc lessen the mass profile.
- The effect of Nb and activation energy enhances the mass profile.
- The fluid temperature also improves with the effect of Biot number, Eckert number, and heat source factor.

Table 2: Numerical outcomes for Sherwood number, skin friction, and Nusselt

Pr	Kc	Nt	Nb	Ec	λ_C	λ_T	Q	m	$f''(\eta)$	$\theta'(\eta)$	$\varphi'(\eta)$
1.0	0.3	0.5	0.5	0.1	0.2	0.1	0.1	0.4	0.028864	0.425904	0.622742
								0,8	0.788763	0.336135	0.562264
								1.2	1.078124	0.324863	0.523164
							0.1	0.4	0.311535	0.141774	0.336641
							0.4		0.164165	0.173934	0.260790
							0.7		0.025644	0.196313	0.285187
							0.1		1.009531	0.316645	0.216600
						0.1			0.749540	0.325513	0.524064
						0.2			0.687721	0.331676	0.431635
					0.2	0.3			0.792933	0.322143	0.322124
					0.4				1.001235	0.323735	0.324013
					0.6				1.010136	0.326832	0.229975
				0.1	0.2				0.621246	0.031698	0.037974
				0.3					0.604724	0.033932	0.032035
				0.5					0.589085	0.031012	0.019921
			0.5	0.1					1.001336	0.323746	0.414074
			1.0						0.795237	0.324243	0.141287
			1.5						0.790535	0.326112	0.056989
		0.5	0.5						0.794236	0.324236	0.141212
		1.0							1.006163	0.321051	0.483309
		1.5							1.006037	0.321809	1.025121
	0.3	0.5							0.685524	0.322121	0.522273
	0.5								0.888634	0.320843	0.520836
	0.7								0.785025	0.320154	0.521085
1.0	0.3								0.783963	0.282465	0.588897
2.0									0.788782	0.221309	0.621282
3.0									0.792801	0.309810	0.546144

The current study can be expanded in the future to include more complexity and variables. Some possible directions for future studies may involve:

1) Including more realistic BCs.
2) Scrutinizing different sorts of nano-particulates.
3) Observing the influence of other external factor.
4) Reconnoitering different heat source/sink profiles.

Acknowledgments: The authors thank the KKU research unit for the financial and administrative support under grant number 593 for year 44.

Funding information: The KKU research unit for the financial and administrative support under grant number 593 for year 44.

Author contributions: All authors have accepted responsibility for the entire content of this manuscript and approved its submission.

Conflict of interest: The authors state no conflict of interest.

Data availability statement: All data generated or analysed during this study are included in this published article.

References

[1] Adnan. Heat transfer inspection in [(ZnO-MWCNTs)/water-EG (50: 50)] hnf with thermal radiation ray and convective condition over a Riga surface. Waves in Random and Complex Media. 2022;1–15.

[2] Algehyne EA, Saeed A, Arif M, Bilal M, Kumam P, Galal AM. Gyrotactic microorganism hybrid nanofluid over a Riga plate subject to activation energy and heat source: Numerical approach. Sci Rep. 2023;13(1):13675.

[3] Ali L, Ali B, Asogwa KK, Apsari R. Transient rotating three-dimensional flow of micropolar fluid induced by Riga plate: Finite element approach. Numer Heat Transfer Part A: Appl. 2023;1–14.

[4] Abdul Hakeem AK, Ragupathi P, Saranya S, Ganga B. Three dimensional non-linear radiative nanofluid flow over a Riga plate. J Appl Comput Mech. 2020;6(4):1012–29.

[5] Ishtiaq B, Nadeem S, Abbas N. Theoretical study of two-dimensional unsteady Maxwell fluid flow over a vertical Riga plate under radiation effects. Sci Iran. 2022;29(6):3072–83.

[6] Asogwa KK, Kumar KT, Goud BS, Chohan JS. Significance of nanoparticle shape factor and buoyancy effects on a parabolic motion of

EMHD convective nanofluid past a Riga plate with ramped wall temperature. Eur Phys J Plus. 2023;138(6):1–13.
[7] Adnan, Abbas W, Said NM, Mishra NK, Mahmood Z, Bilal M. Significance of coupled effects of resistive heating and perpendicular magnetic field on heat transfer process of mixed convective flow of ternary nanofluid. J Therm Anal Calorim. 2024;149(2):879–92.
[8] Bani-Fwaz MZ, Adnan A, Mahmood Z, Bilal M, EI-Zahhar AA, Khan I, et al. Computational Investigation of Thermal Process in Radiated Nanofluid Modulation Influenced by Nanoparticles (Al2O3) and Molecular (H2O) Diameters. J Comput Des Eng. 2024;qwae011.
[9] Waqas M, Almutiri MR, Yagoob B, Ahmad H, Bilal M. Numerical analysis of MHD tangent hyperbolic nanofluid flow over a stretching surface subject to heat source/sink. Pramana. 2024;98(1):27.
[10] Hamad NH, Bilal M, Ali A, Eldin SM, Sharaf M, Rahman MU. Energy transfer through third-grade fluid flow across an inclined stretching sheet subject to thermal radiation and Lorentz force. Sci Rep. 2023;13(1):19643.
[11] Asogwa KK, Goud BS, Shah NA, Yook SJ. Rheology of electromagnetohydrodynamic tangent hyperbolic nanofluid over a stretching riga surface featuring dufour effect and activation energy. Sci Rep. 2022;12(1):14602.
[12] Asogwa KK, Khan I. Radiating and electromagnetic nanofluids flow over an exponentially accelerated Riga plate with heat sink. Waves in Random and Complex Media. 2023;1–22.
[13] Faisal M, Asogwa KK, Mabood F, Badruddin IA. Darcy–Forchheimer dynamics of hybrid nanofluid due to a porous Riga surface capitalizing Cattaneo–Christov theory. Numer Heat Transfer Part A Appl. 2023;1–17.
[14] Asghar A, Vrinceanu N, Ying TY, Lund LA, Shah Z, Tirth V. Dual solutions of convective rotating flow of three-dimensional hybrid nanofluid across the linear stretching/shrinking sheet. Alex Eng J. 2023;75:297–312.
[15] Wakif A, Chamkha A, Thumma T, Animasaun IL, Sehaqui R. Thermal radiation and surface roughness effects on the thermo-magneto-hydrodynamic stability of alumina–copper oxide hybrid nanofluids utilizing the generalized Buongiorno's nanofluid model. J Therm Anal Calorim. 2021;143:1201–20.
[16] Jamshed W, Goodarzi M, Prakash M, Nisar KS, Zakarya M, Abdel-Aty AH. Evaluating the unsteady Casson nanofluid over a stretching sheet with solar thermal radiation: An optimal case study. Case Stud Therm Eng. 2021;26:101160.
[17] Abbas A, Ijaz I, Ashraf M, Ahmad H. Combined effects of variable density and thermal radiation on MHD Sakiadis flow. Case Stud Therm Eng. 2021;28:101640.
[18] Yu D, Wang R. An optimal investigation of convective fluid flow suspended by carbon nanotubes and thermal radiation impact. Mathematics. 2022;10(9):1542.
[19] Sneha KN, Mahabaleshwar US, Sharifpur M, Ahmadi MH, Al-Bahrani M. Entropy analysis in MHD CNTS flow due to a stretching surface with thermal radiation and heat source/sink. Mathematics. 2022;10(18):3404.
[20] Salawu SO, Obalalu AM, Shamshuddin MD. Nonlinear solar thermal radiation efficiency and energy optimization for magnetized hybrid Prandtl–Eyring nanoliquid in aircraft. Arab J Sci Eng. 2023;48(3):3061–72.
[21] Faisal M, Mabood F, Asogwa KK, Badruddin IA. On convective heat and mass transport of radiative double diffusive Williamson hybrid nanofluid by a Riga surface. Int J Mod Phys C. 2023;34(8):2350111.
[22] Asogwa KK, Prasad KR, Kumar R, Murtugudde G, Gowda RP. Transient electromagnetohydrodynamic Nanofluid flow traveling through a moving Riga plate subject to radiation and heat absorption. Int J Mod Phys B. 2023;37(17):22350168.
[23] Asghar A, Ying TY, Zaimi WMKAW. Two-dimensional mixed convection and radiative Al2O3-Cu/H2O hybrid nanofluid flow over a vertical exponentially shrinking sheet with partial slip conditions. CFD Lett. 2022;14(3):22–38.
[24] Asghar A, Lund LA, Shah Z, Vrinceanu N, Deebani W, Shutaywi M. Effect of thermal radiation on three-dimensional magnetized rotating flow of a hybrid nanofluid. Nanomaterials. 2022;12(9):1566.
[25] Dolui S, Bhaumik B, De S. Combined effect of induced magnetic field and thermal radiation on ternary hybrid nanofluid flow through an inclined catheterized artery with multiple stenosis. Chem Phys Lett. 2023;811:140209.
[26] Asghar A, Ying TY, Zaimi K. Two-dimensional magnetized mixed convection hybrid nanofluid over a vertical exponentially shrinking sheet by thermal radiation, joule heating, velocity and thermal slip conditions. J Adv Res Fluid Mech Therm Sci. 2022;95(2):159–79.
[27] Haq I, Bilal M, Ahammad NA, Ghoneim ME, Ali A, Weera W. Mixed convection nanofluid flow with heat source and chemical reaction over an inclined irregular surface. ACS Omega. 2022;7(34):30477–85.
[28] Ali U, Gul T, Khan H, Bilal M, Usman M, Shuaib M, et al. Motile microorganisms hybrid nanoliquid flow with the influence of activation energy and heat source over a rotating disc. Nanotechnology. 2023;34(42):425404.
[29] Raizah Z, Alrabaiah H, Bilal M, Junsawang P, Galal AM. Numerical study of non-Darcy hybrid nanofluid flow with the effect of heat source and hall current over a slender extending sheet. Sci Rep. 2022;12(1):16280.
[30] Elangovan K, Subbarao K, Gangadhar K. Entropy minimization for variable viscous couple stress fluid flow over a channel with thermal radiation and heat source/sink. J Therm Anal Calorim. 2022;147(23):13499–507.
[31] Nabwey HA, Rashad AM, Mahdy AEN, Shaaban SM. Thermal conductivity and thermophoretic impacts of micropolar fluid flow by a horizontal absorbent isothermal porous wall with heat source/sink. Mathematics. 2022;10(9):1514.
[32] Maranna T, Mahabaleshwar US, Perez LM, Manca O. Flow of viscoelastic ternary nanofluid over a shrinking porous medium with heat Source/Sink and radiation. Therm Sci Eng Prog. 2023;40:101791.
[33] Hussain SM, Khan U, Zaib A, Ishak A, Sarris IE. Numerical computation of mixed convective entropy optimized in Darcy-Forchheimer flow of cross nanofluids through a vertical flat plate with irregular heat source/sink. Tribol Int. 2023;187:108757.
[34] Adnan, AlBaidani MM, Mishra NK, Ahmad Z, Eldin SM, Haq EU. Numerical study of thermal enhancement in ZnO-SAE50 nanolubricant over a spherical magnetized surface influenced by Newtonian heating and thermal radiation. Case Stud Therm Eng. 2023;45:102917.
[35] Rasool G, Xinhua W, Lund LA, Yashkun U, Wakif A, Asghar A. Dual solutions of unsteady flow of copper-alumina/water based hybrid nanofluid with acute magnetic force and slip condition. Heliyon. 2023;9(12).
[36] Teh YY, Ashgar A. Three dimensional MHD hybrid nanofluid Flow with rotating stretching/shrinking sheet and Joule heating. CFD Lett. 2021;13(8):1–19.

[37] Yasir M, Khan M. Heat source/sink effect in radiative flow of hybrid nanofluid subject to noninertial frame. Numer Heat Transfer Part A: Appl. 2023;1–14.
[38] Yaseen M, Rawat SK, Khan U, Sarris IE, Khan H, Negi AS, et al. Computational analysis of heat and mass transfer flow of wall jet hybrid nanofluid with irregular heat source/sink effects and waste discharge concentration. J Magn Magn Mater. 2023;588:171434.
[39] Lund LA, Asghar A, Rasool G, Yashkun U. Magnetized casson SA-hybrid nanofluid flow over a permeable moving surface with thermal radiation and Joule heating effect. Case Stud Therm Eng. 2023;50:103510.
[40] Nayak MK, Hakeem AA, Makinde OD. Influence of Catteneo-Christov heat flux model on mixed convection flow of third grade nanofluid over an inclined stretched Riga plate. Defect Diffus. 2018;121–34.
[41] Nayak M, Shaw S, Makinde O, Chamkha AJ. Effects of homogenous–heterogeneous reactions on radiative NaCl-CNP nanofluid flow past a convectively heated vertical Riga plate. J Nanofluids. 2018;7:657–67.
[42] Nayak M, Shaw S, Makinde O, Chamkha AJ. Investigation of partial slip and viscous dissipation effects on the radiative tangent hyperbolic nanofluid flow past a vertical permeable Riga plate with internal heating: Bungiorno model. J Nanofluids. 2019;8:51–62.
[43] Vaidya H, Prasad K, Tlili I, Makinde O, Rajashekhar C, Khan SU, et al. Mixed convective nanofluid flow over a non linearly stretched Riga plate. Case Stud Therm Eng. 2021;24:100828.
[44] Shuaib M, Shah RA, Durrani I, Bilal M. Electrokinetic viscous rotating disk flow of Poisson-Nernst-Planck equation for ion transport. J Mol Liq. 2020;313:113412.
[45] Alrabaiah H, Bilal M, Khan MA, Muhammad T, Legas EY. Parametric estimation of gyrotactic microorganism hybrid nanofluid flow between the conical gap of spinning disk-cone apparatus. Sci Rep. 2022;12:1–14.
[46] Assiri TA, Aziz Elsebaee FA, Alqahtani AM, Bilal M, Ali A, Eldin SM. Numerical simulation of energy transfer in radiative hybrid nanofluids flow influenced by second-order chemical reaction and magnetic field. AIP Adv. 2023;13.
[47] Fang T, Zhang J, Zhong Y. Boundary layer flow over a stretching sheet with variable thickness. Appl Math Comput. 2012;218:7241–52.
[48] Prasad K, Vaidya H, Vajravelu K. MHD mixed convection heat transfer over a non-linear slender elastic sheet with variable fluid properties. AMNS. 2017;2:351–66.